nature neuroscience

Input normalization by global feedforward inhibition expands cortical dynamic range

Frédéric Pouille[1,2], Antonia Marin-Burgin[1,2], Hillel Adesnik[1], Bassam V Atallah[1] & Massimo Scanziani[1]

The cortex is sensitive to weak stimuli, but responds to stronger inputs without saturating. The mechanisms that enable this wide range of operation are not fully understood. We found that the amplitude of excitatory synaptic currents necessary to fire rodent pyramidal cells, the threshold excitatory current, increased with stimulus strength. Consequently, the relative contribution of individual afferents in firing a neuron was inversely proportional to the total number of active afferents. Feedforward inhibition, acting homogeneously across pyramidal cells, ensured that threshold excitatory currents increased with stimulus strength. In contrast, heterogeneities in the distribution of excitatory currents in the neuronal population determined the specific set of pyramidal cells recruited. Together, these mechanisms expand the range of afferent input strengths that neuronal populations can represent.

A characteristic of cortical excitatory neurons is their widely divergent axonal projection. This property enables cortical neurons to contact a large number of postsynaptic cells and allows each postsynaptic cell to receive inputs from many presynaptic neurons. In a circuit constructed with this excitatory divergence alone, the number of active presynaptic neurons (input strength) that is sufficient to recruit all neurons in the postsynaptic population is only slightly larger than the input strength required to recruit any postsynaptic neuron at all. In other words, the input range that can be faithfully represented by the postsynaptic population is restricted. For example, if presynaptic neurons connect to a postsynaptic population with a probability of 15%[1] and each postsynaptic cell requires 40 active inputs to be recruited[2], then 2% of the postsynaptic cells would be recruited by the activity of 200 presynaptic neurons and almost all (>99%) would be recruited by simply doubling the number of active presynaptic neurons (as determined by binomial statistics). Thus, in the absence of control mechanisms, small fluctuations in the fraction of presynaptically active neurons results in all-or-none recruitment of the postsynaptic population[3–6] (this all-or-none behavior is qualitatively similar for a wide range of connectivity values and number of inputs necessary to reach threshold). However, both spontaneous and sensory-evoked cortical activity involves large fluctuations in the fraction of active neurons (for example, refs. 7–9). What mechanisms does the cortex use to expand the range of input strengths over which it faithfully responds? One could imagine at least two distinct mechanisms. Reducing the gain of individual neurons (that is, the change in spiking probability as a function of input strength) would allow each neuron in the population to respond over a wider range of input strengths; this gain modulation could be achieved through $GABA_A$ receptor–mediated conductances[10–13]. Alternatively, staggering the recruitment of individual neurons over a wide range of input strengths would allow the population as a whole, rather than individual neurons, to represent a wider input range. This could be achieved by varying the amplitude of the excitatory postsynaptic currents (EPSCs) necessary to reach threshold for spike generation as a function of input strength.

We found that hippocampal and neocortical feedforward inhibitory circuits staggered the recruitment of individual pyramidal cells over a wide range of input strengths. Feedforward inhibition (FFI) acted homogeneously across the postsynaptic population of pyramidal cells to rapidly adjust their excitability to the strength of incoming presynaptic activity. As a result, the amplitude of the EPSC necessary for a pyramidal cell to reach spike threshold was dynamic and varied with the strength of the input. Heterogeneities in the amplitudes of EPSCs across the postsynaptic population determined the specific subset of pyramidal cells that would spike in response to the presynaptic input. Through this coordinated action of direct excitation and FFI, pyramidal cell populations can remain sensitive to weak inputs, but will not saturate in response to stronger activity.

RESULTS

EPSC necessary to spike pyramidal cell is dynamic

We established the range of stimulus strengths over which the CA1 pyramidal cell population responds, that is, the dynamic range. We recorded from individual pyramidal cells in the loose-patch configuration and stimulated Schaffer collaterals over a range of intensities, from those that failed to trigger any spike to those that triggered spikes on every trial (**Fig. 1a**). The relationship between spiking probability of individual pyramidal cells and input strength (input strength is proportional to the number of activated Schaffer collateral; for details see Online Methods and **Supplementary Fig. 1**) was fitted with a sigmoid to interpolate the threshold input strength, where pyramidal cells spiked in 50% of the trials (**Fig. 1a**). The cumulative distribution of threshold input strengths for all recorded pyramidal cells

[1]Howard Hughes Medical Institute and Neurobiology Section, Division of Biology, University of California San Diego, La Jolla, California, USA. [2]These authors contributed equally to this work. Correspondence should be addressed to M.S. (massimo@ucsd.edu).

Received 5 August; accepted 25 September; published online 1 November 2009; doi:10.1038/nn.2441

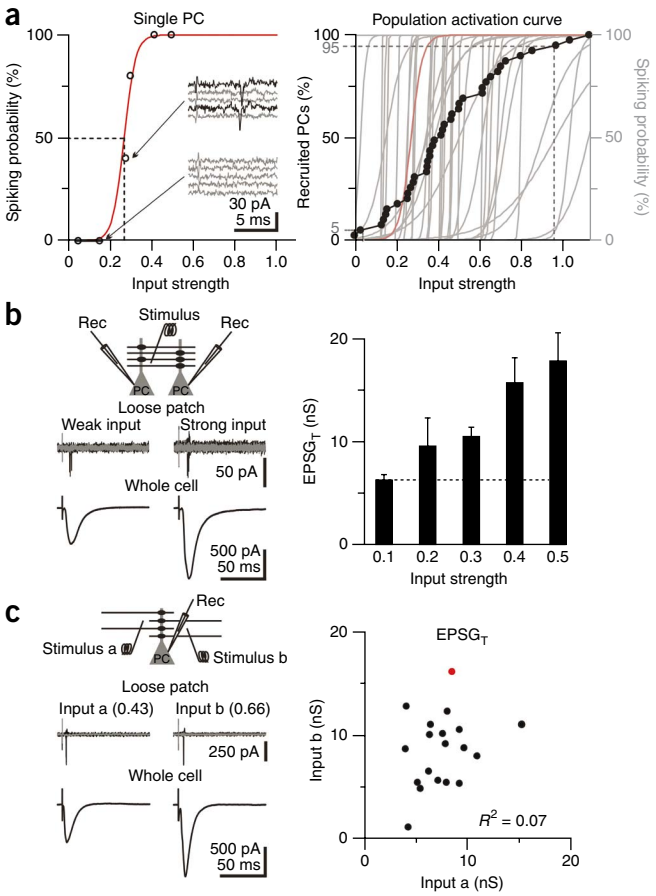

Figure 1 The stronger the stimulus, the larger the excitation necessary to recruit a pyramidal cell. (**a**) Left, spiking probability plotted against input strength for one CA1 pyramidal cell (PC, sigmoidal fit, dashed lines indicate 50% spiking probability). Inset, loose-patch recording at two different input strengths, five consecutive sweeps. Successes are shown in black and failures in gray. Right, black data points represent the activation curve (that is, the cumulative distribution of input strengths eliciting 50% spiking, $n = 39$). Dashed lines represent the input strengths recruiting 5% and 95% of the pyramidal cell population. Gray sigmoids indicate the spiking probability of the 39 pyramidal cells making up the activation curve. Their recruitment was staggered along the range of input strengths. Red sigmoid indicates the experiment shown on the left. (**b**) Top left, recording configuration. Rec, recording electrode. Top traces represent the responses of two CA1 pyramidal cells simultaneously recorded in loose-patch to threshold stimulation of Schaffer collateral inputs (five superimposed sweeps; successes are shown in black, failures in gray). The pyramidal cell on the left was recruited at weaker stimulus than the pyramidal cell on the right. Bottom traces represent threshold EPSCs (that is, EPSCs evoked at threshold input strength, average of ten traces) recorded in the same two cells voltage clamped at –80 mV. The pyramidal cell on the left necessitated less excitation to reach threshold. Right, summary graph of $EPSG_T$s (black, $n = 32$, spike threshold determined in loose patch for $n = 15$ cells and in whole-cell current clamp for $n = 17$ cells) plotted against input strength at threshold (bin width 0.1). Dashed line represents the average $EPSG_T$ for the 0–0.1 bin. Error bars are s.e.m. (**c**) Top left, recording configuration. Top traces represent the response of a single CA1 pyramidal cell recorded in loose patch to threshold stimulation of two different Schaffer collateral inputs (stimuli a and b, five superimposed sweeps each). Bottom traces represent threshold EPSCs (average of ten traces) recorded in the same cell voltage clamped at –90 mV. The difference in amplitude of the two threshold EPSCs should be noted. Right, summary graph ($n = 19$). There was no correlation between $EPSG_T$s evoked by input a and input b (linear regression, $R^2 = 0.07$; spike threshold determined in loose patch for all cells, red data point indicates the experiment shown on the left).

($n = 39$) represents the fractional recruitment of the CA1 pyramidal cell population, or activation curve (**Fig. 1a**). The dynamic range of the pyramidal cell population (that is, the ratio of the input strength necessary to activate 95% versus 5% of the pyramidal cell population) was approximately 34 (**Fig. 1a**), meaning that the pyramidal cell population can differentially represent a 34-fold increase in the number of active Schaffer collateral inputs before saturating. This is much larger than the dynamic range of an individual pyramidal cell (1.6 ± 0.7, $n = 37$; **Fig. 1a**; invariant between pyramidal cells recruited at different input strengths, $R^2 = 0.034$, $P = 0.27$; **Supplementary Fig. 2**) and is the result of staggered recruitment of CA1 pyramidal cells over a wide range of stimulus strengths (**Fig. 1a**).

Why are some pyramidal cells recruited at low input strength, whereas others require much stronger stimuli? We compared the excitatory postsynaptic conductance (EPSG) evoked at threshold input strength[2] of pyramidal cells recruited over the range of input strengths ($EPSG_T$ refers to the EPSG evoked at threshold). **Figure 1b** illustrates an example of two pyramidal cells, simultaneously recorded in the loose-patch configuration, that required different stimulus strengths to spike. Whole-cell, voltage-clamp recording from the same two cells showed that the $EPSG_T$ in the pyramidal cell recruited by the stronger stimulus was much larger than in the pyramidal cell recruited with weaker stimulus (**Fig. 1b**). Over all of the experiments, we observed a steep increase in $EPSG_T$s with increasing input strength (0.3-nS increase per percentile input strength, $n = 32$, $P = 0.0024$; **Fig. 1b**).

The increase in $EPSG_T$ with input strength was not unique to pyramidal cells recruited by single-shock stimulation of the Schaffer collateral. Even when pairs of pyramidal cells were recruited by repetitive high-frequency stimulation (2–6 stimuli at 0.2–0.5 kHz), mimicking bursting activity in CA3, as recorded *in vivo*[14], $EPSG_T$s were significantly larger in the cell recruited with higher input strength (1.7 ± 0.2–fold larger, $n = 12$ pairs, $P = 0.012$; **Supplementary Fig. 3**). This held true for even higher stimulus frequencies (4–6 stimuli at 1 kHz, 1.6 ± 0.2–fold larger, $n = 6$ pairs, $P = 0.045$; **Supplementary Fig. 3**). Thus, pyramidal cells recruited at higher input strengths need larger EPSGs to reach spike threshold.

Are differences in $EPSG_T$ amplitudes the results of variability in intrinsic pyramidal cell properties? Input resistance, membrane time constant, resting potential and threshold potential did not significantly differ between pyramidal cells recruited at different input strengths (**Supplementary Fig. 4**). To further rule out the influence of intrinsic variability between pyramidal cells, we compared $EPSG_T$s between two independent Schaffer collateral inputs converging onto a single pyramidal cell (**Fig. 1c**). $EPSG_T$s were uncorrelated between the two inputs (**Fig. 1c**). Furthermore, in an individual pyramidal cell, the $EPSG_T$ evoked by the stronger input was invariably larger than the $EPSG_T$ evoked by the weaker input (1.5 ± 0.2–fold larger; $P = 0.002$, $n = 19$; **Fig. 1c**). Finally, there was no significant difference in the rise and decay kinetics of $EPSG_T$s evoked by the weak and strong inputs (10–90% rise time: strong stimulus, 2.8 ± 0.2 ms; weak stimulus, 2.6 ± 0.3 ms; $P = 0.67$, $n = 19$; decay time constant: strong stimulus, 7.0 ± 0.4 ms; weak stimulus, 6.8 ± 0.4 ms; $P = 0.74$, $n = 19$), ruling out differences resulting from the distribution of the excitatory inputs along the somatodendritic axis. Thus, even in an individual pyramidal cell, the $EPSG_T$ varied depending on the activated input, indicating that the same pyramidal cell can be recruited at both the low or high end of the stimulus range.

The increase in $EPSG_T$ implies that the contribution of each individual afferent in firing the neuron decreases with increasing input strength. By how much does this decrease? Over the range of

input strengths from 0 to 0.5, the amplitude of the $EPSG_T$ increased approximately linearly (**Fig. 1b**; see model below) such that

$$EPSG_{TN} = Nk + EPSG_{T0}$$

where N is the number of active afferents, $EPSG_{TN}$ is the $EPSG_T$ when N afferents are active, $EPSG_{T0}$ is the EPSG necessary to reach threshold at minimal input strength (under our condition, it was ~6 nS; **Fig. 1b**) and k is the proportionality factor. Given g, the synaptic conductance produced by an individual afferent, the relative contribution of each afferent toward firing a cell, $\left(\frac{g}{EPSG_{TN}}\right)$, is $\frac{g}{(Nk + EPSG_{T0})}$. Thus, the relative contribution of individual afferents in firing a cell is normalized by the number of active afferents.

FFI expands population's dynamic range

What determines the amplitude of the $EPSG_T$ and why does it vary with input strength? Stimulation of Schaffer collaterals triggers powerful FFI in CA1 pyramidal cells through the recruitment of GABAergic interneurons[15–17]. There was a strong correlation between the amplitude of the $EPSG_T$ and the amplitude of the concomitantly triggered feedforward inhibitory postsynaptic conductance (IPSG; **Fig. 2a**; see Online Methods and **Supplementary Fig. 5**). Furthermore, consistent with the correlation between $EPSG_T$ and input strength (**Fig. 1b**), FFI increased with input strength, before saturating at input values above ~0.5 (**Fig. 2a**). These data suggest that $EPSG_T$ may vary with input strength because of a parallel increase of FFI. We directly tested this possibility by either abolishing GABAergic transmission or by imposing a fixed amount of inhibition (**Fig. 2b**). Abolishing FFI with the $GABA_A$ receptor antagonist gabazine eliminated the increase in $EPSG_T$ with input strength (nonsignificant increase of 0.07 nS per percentile input strength, $n = 30$, $P = 0.22$; **Fig. 2b**), demonstrating a crucial role of $GABA_A$ receptors.

To impose a fixed amount of inhibition, irrespective of input strength (**Fig. 2b**), we first inhibited GABA release with the μ-opioid receptor agonist DAMGO (0.5–1 μM, 77.9 ± 7.3% reduction, $n = 4$; **Supplementary Fig. 6**)[18] and then produced a tonic activation of $GABA_A$ receptors by perfusing the selective agonist muscimol (1 μM; average hyperpolarization, −2.4 ± 0.5 mV; average conductance increase, 4.7 ± 0.3 nS; $n = 4$). In the presence of tonic inhibition, $EPSG_T$ no longer varied with input strength (nonsignificant decrease of 0.003 nS per percentile input strength, $n = 14$, $P = 0.4$; **Fig. 2b**). Thus, the progressive increase in $GABA_A$ receptor activation accounts for the increase in $EPSG_T$. This is supported by the fact that at high input strengths (>0.5), when the amplitude of FFI no longer increased (**Fig. 2a**), $EPSG_T$ remained constant (nonsignificant decrease of 0.02 nS per percentile input strength, $P = 0.4$; **Supplementary Fig. 7**).

By how much does the dynamic $EPSG_T$ increase the range of inputs that the pyramidal cell population responds to? We compared the activation curve of the CA1 pyramidal cell population under control conditions and in the presence of gabazine, where the $EPSG_T$ is fixed (**Fig. 2c**). The number of Schaffer collaterals necessary to recruit the lowest fractions of the pyramidal cell population was comparable in both conditions (for example, 5% recruitment: control, 0.028 input strength; gabazine, 0.03 input strength; **Fig. 2c**). The situation was, however, radically different when larger numbers of Schaffer collaterals were activated. In the presence of gabazine, an approximately eightfold increase in the number of activated Schaffer collaterals readily led to the saturation of the pyramidal cell population (95% recruitment with 0.26 input strength), whereas the same increase in stimulated

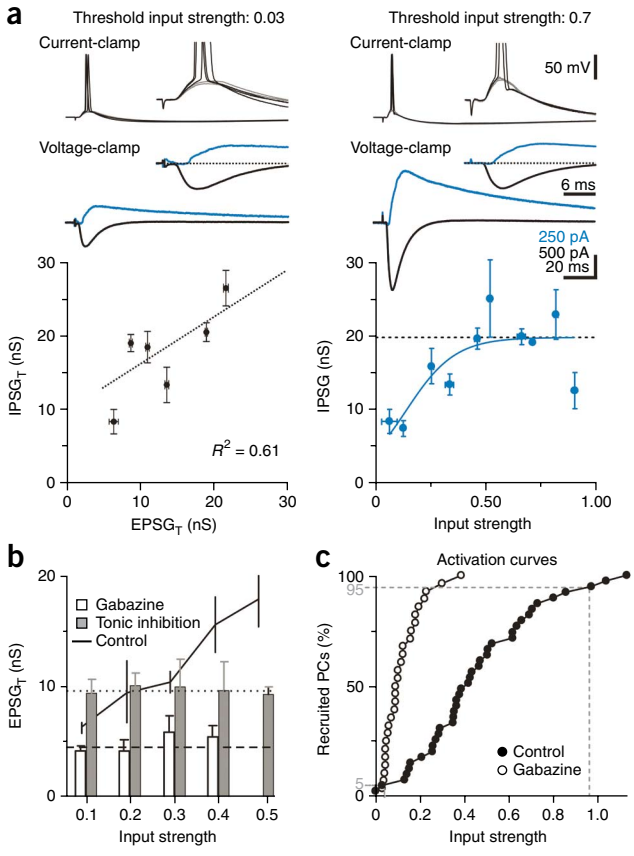

Figure 2 Feedforward inhibition expands the dynamic range of the pyramidal cell population. (**a**) Top traces represent whole-cell current-clamp recording from two CA1 pyramidal cells recruited at threshold by weak (left) or strong (right) Schaffer collateral stimulation (five superimposed sweeps; black indicates successes and gray indicates failures to trigger a spike). Bottom traces, represent threshold EPSC (black, average of five traces recorded in the voltage clamp, –88 and –92 mV for left and right, respectively) and concomitantly evoked feedforward IPSC (blue, recorded at –52 and –59 mV for left and right, respectively, and isolated by subtraction from average of ten sweeps). Insets represent expanded timescale of the sweeps. The size of the two insets has been scaled to match EPSC amplitudes. Bottom left, threshold feedforward IPSG ($IPSG_T$) plotted against $EPSG_T$ (bin width of 2.5 nS, $n = 30$, spike threshold determined in loose patch for $n = 19$ cells and in whole-cell current clamp for $n = 11$ cells, dotted line is the linear regression fit of the binned data, $R^2 = 0.61$, slope of 0.82). Bottom right, feedforward IPSG plotted against input strength (bin width of 0.1, $n = 50$, continuous blue line is a Boltzmann fit of the binned data). Error bars are s.e.m. (**b**) Summary graph of $EPSG_T$s plotted against input strength in the presence of gabazine (6 μM, $n = 30$, spike threshold determined in loose patch for $n = 20$ cells and in whole-cell current clamp for $n = 10$ cells) or under tonic inhibition (1 μM muscimol and 0.5–1 μM DAMGO, $n = 14$, spike threshold determined in loose-patch for $n = 11$ cells and in whole-cell current clamp for $n = 3$ cells). Dotted and dashed horizontal lines represent the average $EPSG_T$ during tonic inhibition or gabazine treatment, respectively. In contrast with control conditions (black line from **Fig. 1b**), the $EPSG_T$ recorded in gabazine or tonic inhibition changed little with increasing input strength. For all input strengths, the $EPSG_T$ during tonic inhibition was larger than during gabazine treatment. (**c**) Activation curves (cumulative distribution of input strengths eliciting 50% spiking) in control conditions (black symbols from **Fig. 1a**) and after gabazine treatment ($n = 28$, spike threshold determined in loose patch for all cells). Dashed lines indicate input strengths recruiting 5% and 95% of the pyramidal cell population. Error bars are s.e.m.

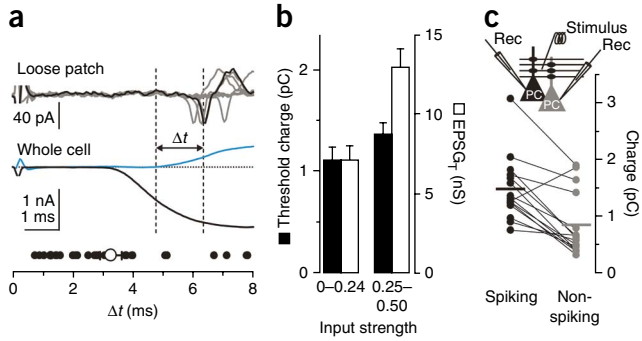

Figure 3 Pyramidal cells spike after the onset of feedforward inhibition. (**a**) Top traces are loose patch recordings from a CA1 pyramidal cell in response to threshold stimulation of Schaffer collaterals (five superimposed sweeps). Bottom traces are voltage-clamp recordings from the same neuron; the EPSC (black line, average of five traces) was recorded at –85 mV and the feedforward IPSC (blue line, isolated by subtraction from average of ten traces) was recorded at –60 mV. The vertical dashed lines mark the onset of the IPSC and the average timing of the spike in the pyramidal cell. The IPSC onset occurred before the spiking of the pyramidal cell. Bottom, summary of 30 similar experiments (spike threshold determined in loose patch for $n = 18$ cells and in whole-cell current clamp for $n = 12$ cells). The open symbol represents the average. (**b**) The net threshold charge (EPSC minus IPSC) entering the cell from the onset of the EPSC to the time of the spike and the $EPSG_T$ are shown for two different ranges of threshold input strengths. The threshold charge did not increase significantly with increasing input strength ($P = 0.3$). In contrast, the peak conductance of the $EPSG_T$ recorded in the same cells was significantly larger for larger input strengths ($P = 0.03$). Error bars represent s.e.m. (**c**) Simultaneous recording from two neighboring pyramidal cells in which Schaffer collaterals stimulation was sufficiently strong to reach threshold in one cell (black), but not in the other (gray, $n = 15$ pairs). The net threshold charge entering in the spiking pyramidal cells was significantly larger than the net charge entering the nonspiking pyramidal cells ($P = 0.004$). Circles represent individual experiments and horizontal lines represent averages.

Schaffer collaterals in control conditions recruited only 19.9% of the population (**Fig. 2c**). Thus, gabazine increased the slope of the activation curve without producing major changes in the offset (**Fig. 2c**). Hence, a dynamic $EPSG_T$ leads to a fourfold expansion of the range of inputs that the CA1 pyramidal cell population can respond to.

FFI arrives before spike

By what mechanism does the feedforward inhibitory postsynaptic current (IPSC) control the size of the $EPSG_T$? We compared the timing of the spike elicited in pyramidal cells by Schaffer collateral stimulation with the onset of the feedforward IPSC. When stimulated at threshold for spike generation, the spike occurred 5.0 ± 0.4 ms after the onset of the EPSC and 3.3 ± 0.4 ms after the onset of the feedforward IPSC ($n = 30$; **Fig. 3a**). The latency between the onset of the EPSC and of the IPSC was 1.65 ± 0.08 ms ($n = 30$), consistent with previous data[15], and did not change with stimulus strength ($R^2 = 0.007$, $P = 0.4$, $n = 30$). Thus, in response to threshold Schaffer collateral stimulation, FFI reached pyramidal cells before the membrane potential of the neuron reached threshold for spike generation.

Over the period preceding the spike, synaptic inhibition overlapped with the EPSC, thereby reducing the excitatory charge entering the cell by 28.1 ± 4.3% ($n = 30$). Specifically, although the integral of the EPSC from its onset to the time of the spike (excitatory charge) averaged 2.2 ± 0.2 pC ($n = 30$), the net synaptic charge (excitatory-inhibitory charge, see Online Methods) entering pyramidal cells was 1.4 ± 0.1 pC ($n = 30$). In contrast to the $EPSG_T$ this net threshold charge was constant and independent of input strength (threshold charge, 1.1 ± 0.1 pC, ($n = 4$) at 0–0.25 input strength versus 1.4 ± 0.1 pC, ($n = 14$) at 0.25–0.5, $P = 0.3$; $EPSG_T$, 7.1 ± 0.9 nS ($n = 4$) at 0–0.25 input strength versus 13.1 ± 1.3 nS ($n = 14$) at 0.25–0.5, $P = 0.03$; **Fig. 3b**). Furthermore, at any given input strength, the threshold charge was significantly larger in pyramidal cells that reached threshold for spike generation as compared with the charge entering over the same time interval in simultaneously recorded cells that did not reach threshold (0.8 ± 0.1 pC, $P = 0.004$, $n = 15$; **Fig. 3c**). In the cells that did not spike, the threshold charge (that is, ~1.5 pC) would have been reached 5.0 ± 0.3 ms after the onset of the EPSC if inhibition had not been present. Thus, by overlapping with excitation before spike occurrence, FFI controls the amplitude of the EPSC necessary to reach spike threshold.

Heterogeneous excitation and homogeneous inhibition

What determines which pyramidal cells in the population are recruited in response to Schaffer collateral stimulation? We recorded from two neighboring pyramidal cells simultaneously (somata separated by ≤50 μm) and increased the number of activated Schaffer collaterals until one of the two cells spiked (**Fig. 4a**). We then compared the EPSGs and feedforward IPSGs in the two cells. Although the EPSG was, on average, 1.6 ± 0.1–fold larger in the cell that spiked ($P = 0.001$, $n = 15$; **Fig. 4b**), the IPSG was, on average, not significantly different between the two neurons (1.1 ± 0.1–fold difference, $P = 0.3$, $n = 15$; **Fig. 4b**). Furthermore, the latency of the feedforward IPSC (with respect to the onset of the EPSC) did not differ significantly between spiking (1.75 ± 0.09 ms) and nonspiking neurons (1.59 ± 0.06 ms, $P = 0.09$, $n = 15$). Thus, differences in the amplitude of synaptic excitation, rather than in the amplitude or timing of inhibition, govern which neuron will spike in response to Schaffer collateral stimulation.

To determine whether inhibition is more homogeneously distributed across pyramidal cells as compared with excitation, we computed the 'spread', that is, the absolute difference in amplitude of simultaneously recorded EPSGs or IPSGs normalized by the average of the amplitudes and divided by two. Although the spread of EPSGs between two simultaneously recorded pyramidal cells was 21 ± 3% ($n = 15$, same paired values as above; **Fig. 4b**), the spread of the concomitant IPSGs was only 11 ± 2% ($P = 0.03$, $n = 15$). We also calculated how well the amplitude of inhibition in one cell correlated with the amplitude of inhibition in its neighbor and did the same for excitation. For this, we used the same paired values as described above (**Fig. 4b**), but we randomly allocated the spiking cell to either one of the two axes (**Fig. 4b**). This randomization removes the correlation bias caused by systematically having the larger amplitude on the same axis. The correlation between IPSGs ($R_{In} = 0.79$) was significantly larger than the correlation between EPSGs ($R_{Ex} = 0.30$, $P < 0.02$, see Online Methods; **Fig. 4b**). Thus, inhibition is more homogeneous than excitation across the pyramidal cell population.

To test whether the relative homogeneity of inhibition with respect to excitation also holds true for individual synaptic events, we compared trial-by-trial fluctuations of the amplitude of EPSC and feedforward IPSC between two simultaneously recorded pyramidal cells (**Fig. 4c**). Using a cesium-based internal solution, we isolated feedforward IPSCs and monosynaptic EPSCs by voltage clamping the cell at the EPSC or IPSC reversal potential, respectively (**Fig. 4c**). The amplitude of the feedforward IPSC covaried between the two recorded neurons (average correlation, $R^2 = 0.26 \pm 0.06$, $n = 5$; **Fig. 4c**). This correlation was significantly less pronounced for monosynaptic EPSCs (average correlation, $R^2 = 0.06 \pm 0.005$, $n = 5$, $P = 0.033$; **Fig. 4c**). These results indicate that, although FFI is

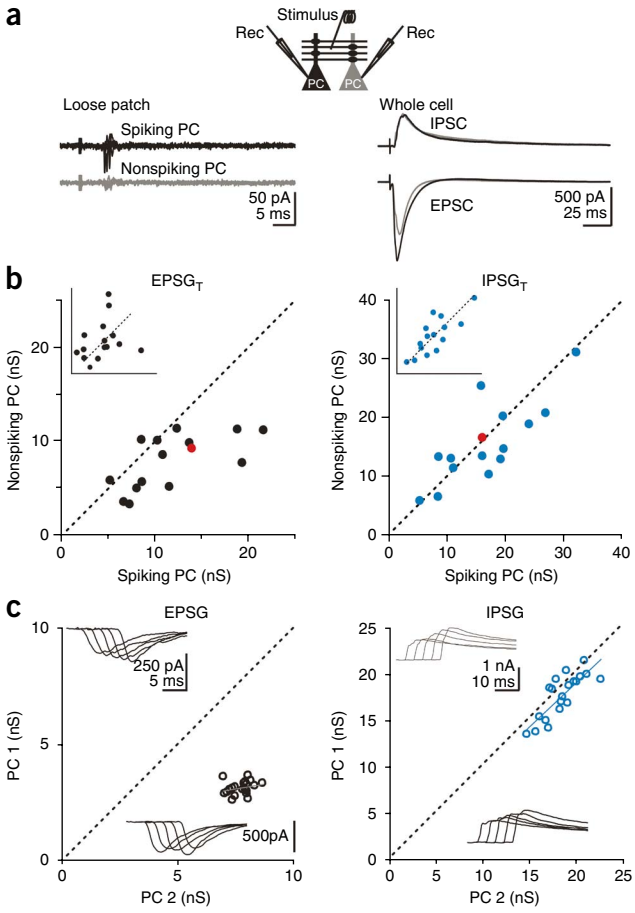

Figure 4 Homogeneous inhibition and heterogeneous excitation control the recruitment of pyramidal cells. (**a**) Top, recording configuration. Left traces represent simultaneous loose-patch recording from two neighboring CA1 pyramidal cells. Schaffer collaterals stimulation was sufficiently strong to reach threshold in one cell (black traces, five superimposed sweeps), but not in the other (gray traces). Right traces represent whole-cell voltage-clamp recording from the same two neurons (top, feedforward IPSCs recorded at –60 mV and isolated by subtraction from average of ten traces; bottom, EPSCs recorded at –80 mV, average of ten traces). The amplitude of the feedforward IPSC was similar in both cells, whereas the EPSC was larger in the cell that spiked. (**b**) Left, summary graph of 15 similar experiments in which the EPSG in the nonspiking cell is plotted against the EPSG in the spiking cell. The majority of the data points are below the unity line (red data point indicates the experiment shown on top). Right, summary graph of the same 15 experiments in which the feedforward IPSG in the nonspiking cell is plotted against the feedforward IPSG in the spiking cell. In contrast with the EPSG, all of the data points are scattered around the unity line (spike threshold determined in loose patch for $n = 8$ pairs and in whole-cell current clamp for $n = 7$ pairs; red data point indicates experiment shown in **a**; same set of experiments illustrated in **Fig. 3c**). Error bars are s.e.m. Insets have the same data points as are shown in the main graphs, but the spiking cell is randomly allocated to either one of the two axes. Note the larger spread of EPSGs as compared with IPSGs. (**c**) Trial-by-trial fluctuation of EPSGs (left) and IPSGs (right) simultaneously recorded in two pyramidal cells (PC 1 and PC 2) voltage clamped at the reversal potential of IPSCs (left) or EPSCs (right, same Schaffer collateral stimulation intensity for both holding potentials, cesium internal). Left, single-trial EPSGs recorded in PC 1 are plotted against the EPSGs recorded simultaneously in PC 2. Upper traces are five example EPSCs recorded in PC 1 ordered according to amplitude. Lower traces are the corresponding five EPSCs recorded simultaneously in PC 2. Right, single-trial IPSGs recorded in PC 1 are plotted against the IPSGs recorded simultaneously in PC 2. Upper traces are five example IPSCs recorded in PC 1 ordered according to amplitude. Lower traces are the corresponding five IPSCs recorded simultaneously in PC 2. Note the marked covariation in amplitude of IPSGs recorded in the two pyramidal cells as compared with EPSGs.

relatively homogenous across the pyramidal cell population, and thus sets a global threshold for pyramidal cell recruitment by Schaffer collaterals, heterogeneities in excitation determine which pyramidal cells in the population overcome this threshold.

Basket cells expand dynamic range of pyramidal cell population

Several types of hippocampal inhibitory interneurons are activated in a feedforward manner[19–22]. What type of interneuron controls the amplitude of the EPSG$_T$ in pyramidal cells? Because the onset of FFI occurs before the spiking of pyramidal cells (see above; **Fig. 3a**), these interneurons must spike before pyramidal cells in response to afferent stimulation. We compared the spike timing of different types of interneurons in response to Schaffer collateral stimulation with the timing of the peak of the population spike (recorded in the stratum pyramidale; **Fig. 5a**,**b**). Pyramidal cells fired simultaneously with the population spike (0.2 ± 0.2 ms, $P = 0.52$, $n = 21$; **Fig. 5a**,**b**), whereas regular-spiking interneurons[19,20] were recruited after the population spike (0.7 ± 0.3 ms, $P = 0.04$, $n = 34$). In contrast, fast-spiking inhibitory interneurons[19,20] fired 1 ± 0.2 ms before the population spike ($P = 0.0003$, $n = 18$; **Fig. 5a**,**b**), consistent with the early onset of FFI. We computed the activation curve of fast-spiking and regular-spiking interneurons (**Fig. 5c**), as we did for pyramidal cells (**Fig. 1a**). The activation curve of fast-spiking interneurons was much steeper that the one for regular-spiking interneurons and pyramidal cells (**Fig. 5c**), consistent with the strong and fast excitation received by fast-spiking interneurons[21,23,24] (half maximal recruitment of fast-spiking interneurons occurred at an input strength of 0.11 compared with 0.37 and 0.4 for regular-spiking interneurons and pyramidal cells, respectively). Notably, the activation curve of fast-spiking interneurons (**Fig. 5c**) provided a good match for the increase in the amplitude of FFI over the same range of stimuli (half maximal recruitment of FFI occurred at an input strength of 0.13; **Fig. 2a**).

Anatomical identification of these fast-spiking interneurons revealed that 63% were basket cells (for axonal and dendritic distribution, see **Supplementary Fig. 8**) and the rest were composed of dendrite targeting interneurons exhibiting axonal arborization consistent with bi-stratified and tri-laminar cells[19,20] ($n = 11$ fast-spiking cells; **Fig. 5a**). Thus, these data indicate that the dynamic EPSG$_T$ in CA1 pyramidal cells is primarily enforced by fast-spiking interneurons, the majority of which are basket cells.

Model

Is the observed change in EPSG$_T$ sufficient to account for the expansion of the range of inputs the pyramidal cell population responds to? We created a simple quantitative model of Schaffer collateral excitation onto a population of CA1 pyramidal cells (**Fig. 6**; see Online Methods). Schaffer collateral inputs contacted pyramidal cells with a probability of 0.06 (ref. 25). We computed the fraction of recruited pyramidal cells as a function of the number of stimulated Schaffer collateral and compared the resulting activation curves under two conditions: with either a fixed or a dynamic EPSG$_T$ (**Fig. 6a**). The threshold to recruit a pyramidal cell was set at 100 Schaffer collateral inputs[2] and remained constant in the fixed EPSG$_T$ condition. In the dynamic EPSG$_T$ condition, the number of Schaffer collaterals necessary to recruit a pyramidal cell increased linearly with increasing number of stimulated Schaffer collaterals, up to approximately threefold,

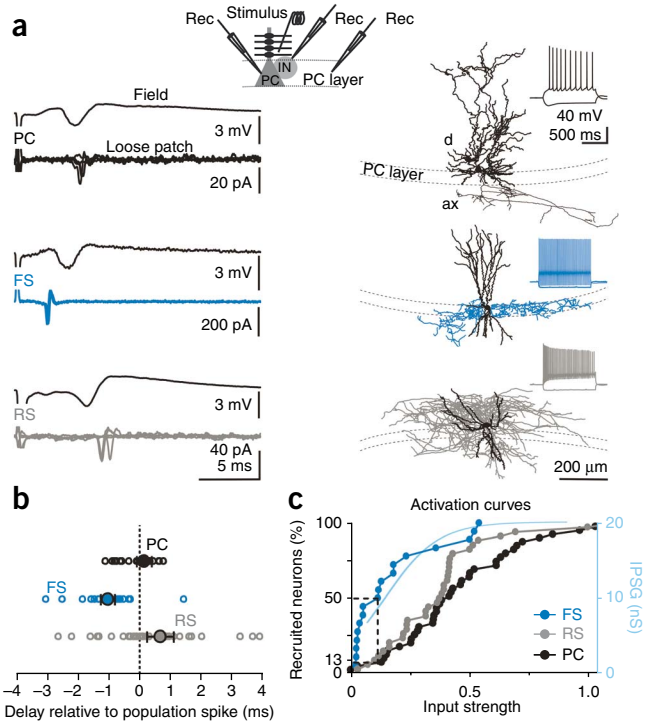

Figure 5 Fast-spiking interneurons enforce dynamic $EPSG_T$. (**a**) Top, recording configuration. Left, simultaneous field (from pyramidal cell layer) and loose-patch recording from three types of neurons in response to Schaffer collateral stimulation (three different experiments): a pyramidal cell (top, five superimposed sweeps), a fast-spiking interneuron (FS, middle, five superimposed sweeps) and a regular-spiking interneuron (RS, bottom, five superimposed sweeps). Although the spike in the pyramidal cell was concomitant with the peak of the population spike recorded with the field electrode, the action potential in the fast-spiking cell preceded, and in the regular-spiking cell followed, the population spike. Right, camera lucida reconstruction of the three neurons on the left (dashed lines mark the margins of the pyramidal cell layer, stratum radiatum is above the dashed lines; d, dendrite; ax, axon). Insets, spiking pattern from same neurons recorded in whole-cell current-clamp configuration in response to depolarizing and hyperpolarizing current steps. (**b**) Relative timing of spikes elicited in response to Schaffer collateral stimulation in pyramidal cells (black, $n = 21$), fast-spiking interneurons (blue, $n = 18$) and regular-spiking interneurons (gray, $n = 34$) with respect to the peak of population spike (spike threshold determined in loose patch for all cells). On average, fast-spiking interneurons fired before and regular-spiking interneurons fired after the population spike. (**c**) Activation curves (cumulative distribution of threshold input strengths) for fast-spiking (blue, $n = 18$), regular-spiking (gray, $n = 34$) and pyramidal cells (black, $n = 39$, from **Fig. 1a**). The input strength that recruited 50% of fast-spiking interneurons elicited spikes in only 13% of pyramidal cells (spike threshold determined in loose patch for all cells). The continuous light blue line is the fit of the feedforward IPSG as a function of input strength (right ordinate from **Fig. 2a**, asymptote scaled to 100%). There was a good match with the activation curve of fast-spiking neurons.

and then remained constant to simulate experimental observation (**Fig. 6b**). The exact increment of the modeled dynamic $EPSG_T$ was chosen to yield an activation curve that best approximated the experimentally observed activation curve (**Fig. 6c**). With a fixed $EPSG_T$, the activation curve was steep and had a narrow dynamic range (**Fig. 6c**). With a dynamic $EPSG_T$, on the other hand, the activation curve had an onset similar to the fixed threshold activation curve, but rose much less steeply, resulting in a wider dynamic range (**Fig. 6c**; the sensitivity of the slope of the activation curve to the rate of increase of the dynamic $EPSG_T$ is illustrated in **Supplementary Fig. 9**).

The dynamic $EPSG_T$ activation curve (**Fig. 6c**) is the synthesis of a family of fixed $EPSG_T$ activation curves, each having progressively larger $EPSG_T$ (a subset are illustrated in **Fig. 6c**). An intersection occurs at the specific input strength at which dynamic and fixed $EPSG_T$ activation curves have equal $EPSG_T$.

This simple model captures the basic experimental finding, namely that the dynamic $EPSG_T$ expands the range of inputs that the CA1 pyramidal cell population responds to by maintaining sensitivity to weak inputs and preventing saturation to stronger stimuli. It should be noted, however, that the modeled fixed and dynamic $EPSG_T$ activation curves both fail to fully account for the experimentally observed activation curves, where more than ~80% of pyramidal cells are active (see Discussion).

Dynamic $EPSG_T$ in somatosensory cortex

Feedforward inhibitory circuits involving fast-spiking interneurons have been described along several cortical projections[24,26–29]. Is the dynamic $EPSG_T$ a general mechanism by which the cortex expands the range of inputs it can respond to? We tested this hypothesis at one of the main projections in the neocortical 'canonical circuit', the

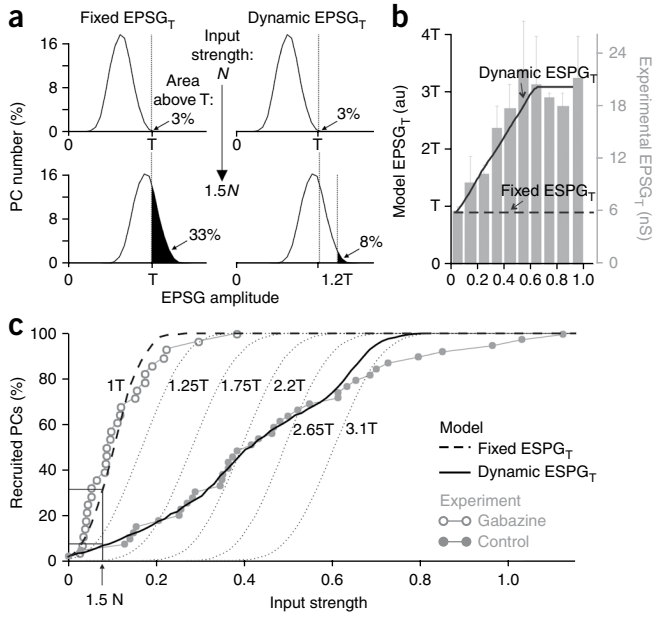

Figure 6 Model of activation curve with dynamic $EPSG_T$. (**a**) Modeled distribution of EPSG amplitudes in the population of pyramidal cells when N (top row) and $1.5N$ (bottom) afferent fibers are active. The area above spike threshold T, under the curve (black shaded), is the fraction of pyramidal cells recruited with either fixed (left column) or dynamic (right) $EPSG_T$. For dynamic $EPSG_T$, a smaller fraction of pyramidal cells was recruited when increasing the number of active afferent fibers from N to $1.5N$. (**b**) $EPSG_T$ as a function of input strength used in the model; dynamic (continuous line), fixed (dashed line) and experimentally measured dynamic $EPSG_T$ (gray columns, same data as in **Fig. 1**, but for the entire range of stimulus strengths) are shown. (**c**) Modeled pyramidal cell activation curves with fixed or dynamic $EPSG_T$. Experimentally measured activation curve in gabazine and control conditions are superimposed. Dotted gray lines represent a set of fixed $EPSG_T$ activation curves (for each activation curve, the threshold is given in multiples of T, the threshold at minimal input strength). The dynamic $EPSG_T$ activation curve intersects each of the fixed $EPSG_T$ activation curves at the specific input strength at which the threshold of the two curves matches. The dynamic $EPSG_T$ activation curve thus results from the synthesis of a family of fixed $EPSG_T$ activation curves.

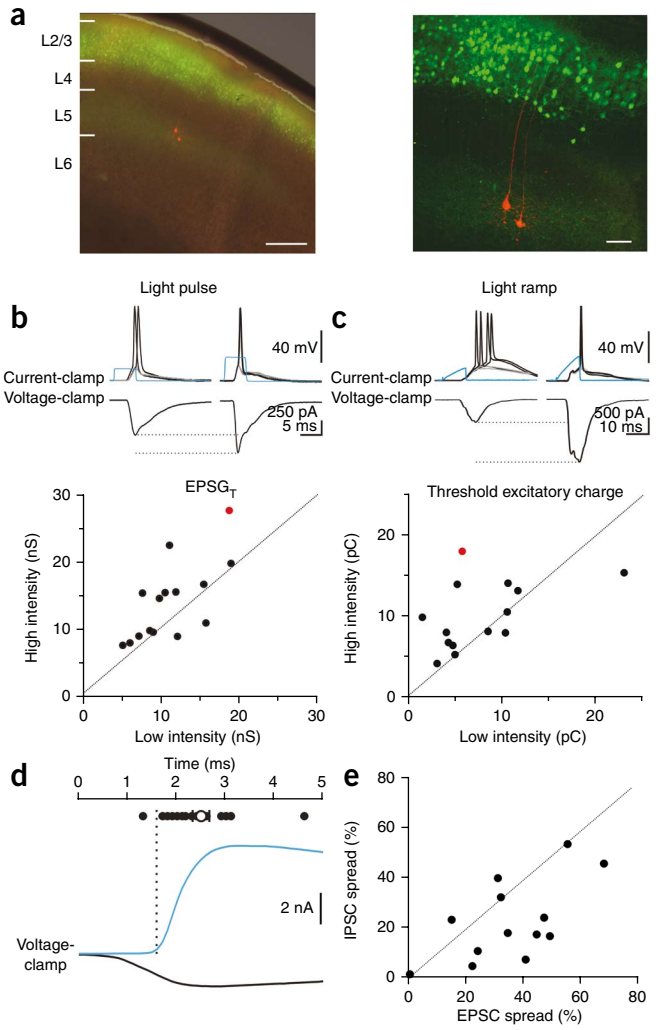

Figure 7 The stronger the photostimulation of L2/3 pyramidal cells, the larger the excitation necessary to recruit L5 pyramidal cells. (**a**) Left, overlay of low-magnification bright-field and red and green fluorescent images of a representative cortical brain slice from a 27-day-old mouse electroporated while *in utero* with ChR2-Venus (green). The red cells are a pair of L5 pyramids filled with Alexa Fluor 568. Note the green band of ChR2-Venus–expressing cells in L2/3 and the fainter band in L5 representing the axonal arborization of the L2/3-L5 projection. Scale bar represents 200 μm. Right, two-photon stack of the same slice at higher magnification. Scale bar represents 50 μm. Nearly all of the ChR2-Venus–expressing neurons were in L2/3. Individual axons from L2/3 cells can be seen crossing L4 and arborizing in L5. (**b**) Top, simultaneous current-clamp recording from two layer 5 pyramidal cells excited by a 5-ms square light pulse. The pyramidal cell on the left was recruited at threshold by lower-intensity photostimulation as compared with the pyramidal cell on the right. Successes in triggering a spike are shown in black and failures in gray (3–4 superimposed traces). The blue traces indicate the duration and relative amplitudes of the photostimulations. Bottom traces, threshold EPSCs (average of 5–10 traces) recorded in the same two cells voltage clamped at −70 mV. The pyramidal cell on the left necessitated less excitation to reach threshold. A summary graph of EPSG$_T$s recorded in cells recruited by the higher-intensity photostimulus plotted against the EPSG$_T$ simultaneously recorded in cells recruited by the lower-intensity photostimulus ($n = 15$) is shown. Most of the data points lie above the unity line (red data point indicates the experiment shown on top). (**c**) The same experimental configuration as in **b** was used, but photostimulation is a 10-ms light ramp. The scatter plot shows the threshold excitatory charge (threshold EPSC time integral) recorded in cells recruited by the higher-intensity photostimulus plotted against the threshold excitatory charge simultaneously recorded in cells recruited by the lower-intensity photostimulus ($n = 14$). As in **b**, most of the data points lie above the unity line (red data point indicates the experiment shown on top). (**d**) Top, plot of spike latencies of L5 pyramidal cells to stimulation of L2/3 with 5-ms pulses of blue light (black symbols). Bottom, EPSC (black trace, recorded at IPSC reversal potential) and IPSC (blue trace, recorded at EPSC reversal potential) in a layer 5 pyramidal cell with a cesium-based internal solution. The onset of disynaptic inhibition (5% of peak, vertical dotted line) preceded the average spike latency (open symbol). Error bars are s.e.m. (**e**) Scatter plot of the spread of EPSCs plotted against the spread of IPSCs recorded in pairs of L5 neurons. Most data-point are below the unity line ($n = 13$ pairs).

layer 2/3 to layer 5 excitatory projection of the somatosensory cortex[1] (**Fig. 7**). Because cortical architecture does not permit selective stimulation of the axons of layer 2/3 pyramidal cells with an extracellular stimulation electrode, we electroporated mice *in utero* with channelrhodopsin-2 (ChR2) to target layer 2/3 pyramidal cell progenitors[30,31] (**Fig. 7a**; see Online Methods). Photoactivation of ChR2-expressing layer 2/3 pyramidal cells in slices of juvenile brains triggered both direct excitation and FFI in layer 5 pyramidal cells (**Supplementary Fig. 10**). We recorded from two postsynaptic layer 5 pyramidal cells simultaneously and increased the intensity of the photostimulation of the layer 2/3 axons until one of the two recorded layer 5 pyramidal cells reached spike threshold (low-intensity stimulation). We then further increased the intensity of the photostimulation until the second layer 5 pyramidal cell reached threshold (high-intensity stimulation). Similar to the hippocampus, layer 5 pyramidal cells recruited at high intensity required larger EPSG$_T$s as compared with pyramidal cell recruited at low intensity (1.3 ± 0.1–fold more, $n = 15$, $P = 0.019$; **Fig. 7b**). This difference in EPSG$_T$ was not a result of differences in membrane properties of layer 5 pyramidal cells (input resistance: low-intensity cells, 92 ± 14 MΩ; high-intensity cells, 94 ± 14 MΩ; $P = 0.90$, $n = 15$; membrane time constant: low-intensity cells, 19 ± 2 ms; high-intensity cells, 21 ± 2 ms; $P = 0.41$, $n = 15$).

Does the EPSG$_T$ also vary when afferent activity is distributed in time, similar to what occurs under more physiological conditions[7]? To desynchronize the activation of the input population, we progressively ramped up the intensity of the light stimulus over a period of 10 ms (**Fig. 7c**; see Online Methods). When recording from two layer 5 pyramidal cells simultaneously, as described above, the excitatory charge necessary to recruit the layer 5 pyramidal cell with the high-intensity stimulus was 1.8 ± 0.4–fold larger than for pyramidal cells recruited at low intensity ($n = 14$, $P = 0.021$; **Fig. 7c**). This indicates that the EPSG$_T$ also varies under conditions in which the activity of presynaptic neurons is desynchronized. Thus, the EPSG$_T$ is dynamic for layer 5 cortical pyramidal cells, such that a pyramidal cell recruited when many presynaptic layer 2/3 pyramidal cells are active necessitates significantly larger EPSGs than a pyramidal cell recruited when few layer 2/3 pyramidal cells are active. Is the dynamic EPSG$_T$ in the somatosensory cortex based on the same mechanism as the one identified in the hippocampus? As in the hippocampus, the onset of FFI preceded the spiking of layer 5 pyramidal cells (by 2.0 ± 0.4 ms, $n = 24$; **Fig. 7d**) and increased with stimulus strength (**Supplementary Fig. 10**). The overlap between EPSC and IPSC before spike generation was even more pronounced in response to desynchronized activation of the inputs. In fact, although the latency between EPSC and feedforward IPSC was similar to what we observed in response to a synchronized stimulus (1.5 ± 0.1 ms, $n = 3$), the spiking occurred only 6.2 ± 0.1 ms ($n = 26$) after the onset of the EPSC, resulting in an almost 5-ms overlap. Finally, similar to the hippocampus,

FFI appeared to be more homogenously distributed across layer 5 pyramidal cells as compared with excitation. Although the spread of the EPSCs simultaneously recorded in two pyramidal cells was 36 ± 5% (n = 13), the spread of the concomitant IPSCs was 23 ± 4% (P = 0.007, n = 13; **Fig. 7e**).

DISCUSSION

Our data suggest that the EPSC amplitude necessary to reach spike threshold in hippocampal and neocortical pyramidal cells is dynamic and increases when the number of active neurons in the presynaptic layer increases. Accordingly, the fractional contribution of an individual afferent input in firing a neuron is not fixed, but instead is continuously normalized by the total number of active afferents. Through this simple mechanism, the pyramidal cell population can smoothly operate over a wide range of stimulus strengths. This mechanism is probably important for enabling cortical structures such as the hippocampus to be responsive to weak stimuli, but remain sparsely active even when confronted with stronger inputs. Although FFI sets a global threshold for recruitment of pyramidal cells, local differences in afferent excitation determine which pyramidal cell is recruited.

The fraction of neurons active at any given moment in cortical areas strongly fluctuates as a result of either varying sensory stimuli or ongoing intrinsic activity. The probability of spiking in layer 2/3 pyramidal cells in the somatosensory cortex, for example, rapidly fluctuates in response to naturalistic stimuli applied to the whiskers[7]. Similarly, activity levels in the hippocampus can vary from sparse activity in the exploring animal[8] to synchronous activation of a large fraction of neurons during ripples[9]. As a consequence, downstream targets of these neuronal populations experiences substantial fluctuations in the fraction of afferents that are active at any given time point. The connectivity patterns of cortical excitatory projections, however, are ill-suited to allow postsynaptic populations of neurons to operate over a wide range of afferent activity[5]; afferent axons typically form very divergent projections to contact a large number of postsynaptic targets through relatively weak contacts, such that the simultaneous activity of several afferents is necessary to recruit a target neuron[2,32]. Because of this divergence, gradual increases in the number of active afferents produce very steep, or explosive, increases in the fraction of recruited targets[5], resulting in a limited range of input strengths that can be differentially represented by the postsynaptic population.

Our data indicate that paleo- and neocortical circuits expand the range of afferent input strengths that the cells can respond to by ensuring that, when the input is strong, pyramidal cells necessitate larger EPSCs to reach thresholds. The dynamic range of the population is several-fold wider than the dynamic range of an individual pyramidal cell (34 versus 2). Neither the dynamic range nor the gain (slope of the sigmoidal fit, R^2 = 0.046, P = 0.2) of individual pyramidal cells varied between pyramidal cells recruited along the entire input range. Thus, although $GABA_A$ receptor–mediated conductances can regulate the gain of individual neurons[10–12], our data suggest that pyramidal cell populations can function over a wide range of afferent intensities without requiring gain changes in individual neurons.

Individual excitatory afferent inputs to cortical areas diverge to contact fast-spiking basket cells and principal neurons. The match between the increase in FFI and the activation curve of fast-spiking cells (**Fig. 5c**) suggests that the increase in FFI results from the increased fraction of recruited fast-spiking cells. Because fast-spiking basket cells receive larger and faster EPSPs[21,24,26], they were recruited before pyramidal cells in response to afferent activity (**Fig. 3**)[33]. This led to a substantial temporal overlap between EPSCs and FFI before spike generation in pyramidal cells (**Fig. 3**). Only those pyramidal cells that received large enough EPSCs to overcome the concomitantly occurring inhibition reached spike threshold. With increasing stimulus strength, the amplitude of FFI increased (**Fig. 2a**) and larger EPSCs became necessary for pyramidal cells to reach spike threshold. The onset of inhibition before spike generation in pyramidal cells also means that this early phase of inhibition is unlikely to be of feedback origin, as feedback inhibition is a consequence of pyramidal cell spiking. The control of the amplitude of the EPSC necessary to reach threshold by FFI is likely to be even more marked in response to repetitive, burst-like[14] or asynchronous afferent activity, as a result of the large temporal overlap between afferent excitation and FFI generated by the previous stimulus. Whether the activation curve of fast-spiking cells (**Fig. 5c**) is also controlled by inhibitory inputs remains to be established. If so, reciprocal inhibition of fast-spiking cells may influence the dynamic range of pyramidal cell populations.

Our model captures the initial 80% of the activation curve; that is, until the $EPSG_T$ plateaus above input strength of ~0.5. At these greater input strengths, the $EPSG_T$ is fixed and the model predicts that the activation curve behaves accordingly. However, the top 20% of the experimentally determined activation curve extends beyond this prediction. It is possible that the observed onset of the plateau is inaccurate because of an error in measurement (for example, the lack of proper voltage clamp) and that the real $EPSG_T$ continues to grow with increasing input strength. Alternatively, a small portion of pyramidal cells may receive Schaffer collateral inputs with very low probability as compared with the rest of the population (resulting from heterogeneity in the population or damage to their dendrites) such that they necessitate a much larger stimulus strength to be recruited. Our model also illustrates the fact that the activation curve is sensitive to how steeply the $EPSG_T$ varies with input strength. Because the increase in $EPSG_T$ is, at least in part, determined by the increase in FFI, any parameter that controls the excitability of GABAergic interneurons, such as neuromodulators, will probably affect the slope of the activation curve, and thus the range of input strength that can be represented by the postsynaptic pyramidal cell population.

What determines the specific pattern of pyramidal cells recruited by a stimulus? We found distinct roles for excitation and FFI; a relatively homogeneous inhibition across pyramidal cells sets a global threshold[34] that is proportional to stimulus strength and heterogeneities in excitation determine the precise pattern of pyramidal cells recruited in that population. The situation *in vivo* may create additional biases; through the local action of neuromodulators, such as acetylcholine, some pyramidal cells may be more depolarized than others and reach spike threshold even if they receive less excitation than their neighbors. The local action of presynaptic inhibitors of GABA release, such as opiates, cannabinoids or GABA itself, may create spatial heterogeneities in inhibition that were not present in the slice. Several synaptic and connectivity properties may contribute to homogeneous distribution of FFI, including the strong divergence of individual fast-spiking cells onto the pyramidal cell population[21,35–37], the large number of contacts made by individual fast-spiking cells onto each pyramidal cell[38] and the relatively large number of recruited fast-spiking cells even at low stimulus strength (**Fig. 5c**).

In summary, because the $EPSG_T$ is controlled in a feedforward manner, the sensitivity of pyramidal cells is virtually instantaneously adjusted to match the strength of the afferent stimulus. This instantaneous adjustment differs from adaptation because it does not rely on the previous history of the network through a negative feedback mechanism, such as feedback inhibition, spike adaptation, synaptic depression or presynaptic inhibition. The presence of feedforward inhibitory circuits along several major excitatory pathways

in the brain[15,16,29,39,40] suggests that the expansion of the dynamic range by instantaneously varying the amplitude of the EPSC necessary to reach threshold may not be unique to hippocampus and somatosensory cortex.

METHODS

Methods and any associated references are available in the online version of the paper at http://www.nature.com/natureneuroscience/.

Note: Supplementary information is available on the Nature Neuroscience website.

ACKNOWLEDGMENTS

We thank P. Abelkop for anatomical reconstructions of biocytin filled neurons, F. Fröhlich for developing the initial versions of model, M. Carandini and J. Isaacson for comments and suggestions during the entire course of the project, C. Poo and F. Bertaso for inputs on the manuscript, and all of the members of the Scanziani laboratory for their input on the project and the manuscript. M.S. thanks C. Staub for the original discussions leading to the project. This work was funded in part by the US National Institutes of Health (MH71401 to M.S. and NS061521 to B.V.A.). H.A. is a fellow of the Helen Hay Whithney Foundation. M.S. is an investigator of the Howard Hughes Medical Institute.

AUTHOR CONTRIBUTIONS

F.P. and A.M.-B. conducted the experiments in the hippocampus; H.A. conducted the experiments in the somatosensory cortex; B.V.A. made the model; and M.S. supervised the project and wrote the manuscript.

Published online at http://www.nature.com/natureneuroscience/.
Reprints and permissions information is available online at http://www.nature.com/reprintsandpermissions/.

1. Lefort, S., Tomm, C., Floyd Sarria, J.C. & Petersen, C.C. The excitatory neuronal network of the C2 barrel column in mouse primary somatosensory cortex. *Neuron* **61**, 301–316 (2009).
2. Otmakhov, N., Shirke, A.M. & Malinow, R. Measuring the impact of probabilistic transmission on neuronal output. *Neuron* **10**, 1101–1111 (1993).
3. Marr, D. A theory of cerebellar cortex. *J. Physiol. (Lond.)* **202**, 437–470 (1969).
4. Vogels, T.P. & Abbott, L.F. Signal propagation and logic gating in networks of integrate-and-fire neurons. *J. Neurosci.* **25**, 10786–10795 (2005).
5. Shadlen, M.N. & Newsome, W.T. The variable discharge of cortical neurons: implications for connectivity, computation and information coding. *J. Neurosci.* **18**, 3870–3896 (1998).
6. Diesmann, M., Gewaltig, M.O. & Aertsen, A. Stable propagation of synchronous spiking in cortical neural networks. *Nature* **402**, 529–533 (1999).
7. Arabzadeh, E., Zorzin, E. & Diamond, M.E. Neuronal encoding of texture in the whisker sensory pathway. *PLoS Biol.* **3**, e17 (2005).
8. Wilson, M.A. & McNaughton, B.L. Dynamics of the hippocampal ensemble code for space. *Science* **261**, 1055–1058 (1993).
9. Csicsvari, J., Hirase, H., Mamiya, A. & Buzsaki, G. Ensemble patterns of hippocampal CA3–CA1 neurons during sharp wave–associated population events. *Neuron* **28**, 585–594 (2000).
10. Shu, Y., Hasenstaub, A., Badoual, M., Bal, T. & McCormick, D.A. Barrages of synaptic activity control the gain and sensitivity of cortical neurons. *J. Neurosci.* **23**, 10388–10401 (2003).
11. Mitchell, S.J. & Silver, R.A. Shunting inhibition modulates neuronal gain during synaptic excitation. *Neuron* **38**, 433–445 (2003).
12. Chance, F.S., Abbott, L.F. & Reyes, A.D. Gain modulation from background synaptic input. *Neuron* **35**, 773–782 (2002).
13. Carvalho, T.P. & Buonomano, D.V. Differential effects of excitatory and inhibitory plasticity on synaptically driven neuronal input-output functions. *Neuron* **61**, 774–785 (2009).
14. Tropp Sneider, J., Chrobak, J.J., Quirk, M.C., Oler, J.A. & Markus, E.J. Differential behavioral state-dependence in the burst properties of CA3 and CA1 neurons. *Neuroscience* **141**, 1665–1677 (2006).
15. Pouille, F. & Scanziani, M. Enforcement of temporal fidelity in pyramidal cells by somatic feedforward inhibition. *Science* **293**, 1159–1163 (2001).
16. Buzsáki, G. Feed-forward inhibition in the hippocampal formation. *Prog. Neurobiol.* **22**, 131–153 (1984).
17. Alger, B.E. & Nicoll, R.A. Feed-forward dendritic inhibition in rat hippocampal pyramidal cells studied *in vitro*. *J. Physiol. (Lond.)* **328**, 105–123 (1982).
18. Nicoll, R.A., Alger, B.E. & Jahr, C.E. Enkephalin blocks inhibitory pathways in the vertebrate CNS. *Nature* **287**, 22–25 (1980).
19. Somogyi, P. & Klausberger, T. Defined types of cortical interneurone structure space and spike timing in the hippocampus. *J. Physiol. (Lond.)* **562**, 9–26 (2005).
20. Freund, T.F. & Buzsáki, G. Interneurons of the hippocampus. *Hippocampus* **6**, 347–470 (1996).
21. Glickfeld, L.L. & Scanziani, M. Distinct timing in the activity of cannabinoid-sensitive and cannabinoid-insensitive basket cells. *Nat. Neurosci.* **9**, 807–815 (2006).
22. Maccaferri, G. & Dingledine, R. Control of feedforward dendritic inhibition by NMDA receptor–dependent spike timing in hippocampal interneurons. *J. Neurosci.* **22**, 5462–5472 (2002).
23. Geiger, J.R., Lubke, J., Roth, A., Frotscher, M. & Jonas, P. Submillisecond AMPA receptor–mediated signaling at a principal neuron-interneuron synapse. *Neuron* **18**, 1009–1023 (1997).
24. Cruikshank, S.J., Lewis, T.J. & Connors, B.W. Synaptic basis for intense thalamocortical activation of feedforward inhibitory cells in neocortex. *Nat. Neurosci.* **10**, 462–468 (2007).
25. Sayer, R.J., Friedlander, M.J. & Redman, S.J. The time course and amplitude of EPSPs evoked at synapses between pairs of CA3/CA1 neurons in the hippocampal slice. *J. Neurosci.* **10**, 826–836 (1990).
26. Gabernet, L., Jadhav, S.P., Feldman, D.E., Carandini, M. & Scanziani, M. Somatosensory integration controlled by dynamic thalamocortical feed-forward inhibition. *Neuron* **48**, 315–327 (2005).
27. Helmstaedter, M., Staiger, J.F., Sakmann, B. & Feldmeyer, D. Efficient recruitment of layer 2/3 interneurons by layer 4 input in single columns of rat somatosensory cortex. *J. Neurosci.* **28**, 8273–8284 (2008).
28. Daw, M.I., Ashby, M.C. & Isaac, J.T. Coordinated developmental recruitment of latent fast spiking interneurons in layer IV barrel cortex. *Nat. Neurosci.* **10**, 453–461 (2007).
29. Mittmann, W., Koch, U. & Hausser, M. Feed-forward inhibition shapes the spike output of cerebellar Purkinje cells. *J. Physiol. (Lond.)* **563**, 369–378 (2005).
30. Saito, T. & Nakatsuji, N. Efficient gene transfer into the embryonic mouse brain using *in vivo* electroporation. *Dev. Biol.* **240**, 237–246 (2001).
31. Petreanu, L., Huber, D., Sobczyk, A. & Svoboda, K. Channelrhodopsin-2–assisted circuit mapping of long-range callosal projections. *Nat. Neurosci.* **10**, 663–668 (2007).
32. Bruno, R.M. & Sakmann, B. Cortex is driven by weak, but synchronously active, thalamocortical synapses. *Science* **312**, 1622–1627 (2006).
33. Porter, J.T., Johnson, C.K. & Agmon, A. Diverse types of interneurons generate thalamus-evoked feedforward inhibition in the mouse barrel cortex. *J. Neurosci.* **21**, 2699–2710 (2001).
34. Poo, C. & Isaacson, J.S. Odor representations in olfactory cortex: "sparse" coding, global inhibition and oscillations. *Neuron* **62**, 850–861 (2009).
35. Holmgren, C., Harkany, T., Svennenfors, B. & Zilberter, Y. Pyramidal cell communication within local networks in layer 2/3 of rat neocortex. *J. Physiol. (Lond.)* **551**, 139–153 (2003).
36. Beierlein, M., Gibson, J.R. & Connors, B.W. Two dynamically distinct inhibitory networks in layer 4 of the neocortex. *J. Neurophysiol.* **90**, 2987–3000 (2003).
37. Thomson, A.M., West, D.C., Wang, Y. & Bannister, A.P. Synaptic connections and small circuits involving excitatory and inhibitory neurons in layers 2–5 of adult rat and cat neocortex: triple intracellular recordings and biocytin labeling *in vitro*. *Cereb. Cortex* **12**, 936–953 (2002).
38. Buhl, E.H., Halasy, K. & Somogyi, P. Diverse sources of hippocampal unitary inhibitory postsynaptic potentials and the number of synaptic release sites. *Nature* **368**, 823–828 (1994).
39. Blitz, D.M. & Regehr, W.G. Timing and specificity of feed-forward inhibition within the LGN. *Neuron* **45**, 917–928 (2005).
40. Agmon, A. & Connors, B.W. Thalamocortical responses of mouse somatosensory (barrel) cortex *in vitro*. *Neuroscience* **41**, 365–379 (1991).

ONLINE METHODS

All experiments were conducted in accordance with the animal use guidelines set out by the Institutional Animal Care and Use Committee of the University of California, San Diego.

Slice preparation. Acute hippocampal slices (400 μm) were prepared from 4–5-week-old male Wistar rats and incubated for 45 min in an interface chamber at 34 °C in normal artificial cerebrospinal fluid (ACSF) containing 119 mM NaCl, 2.5 mM KCl, 1.3 mM NaH_2PO_4, 1.3 mM $MgCl_2$, 2.5 mM $CaCl_2$, 26 mM $NaHCO_3$ and 11 mM glucose (equilibrated with 95% O_2 and 5% CO_2). The slices were kept at room temperature (20–25 °C) for 0 to 6 h before being placed in a submerged chamber for recording at 31–33 °C.

Coronal slices (400 μm) from somatosensory cortex were prepared from postnatal day 15–25 ICR white mice in modified ACSF containing 83 mM NaCl, 2.5 mM KCl, 1.0 mM NaH_2PO_4, 3.3 mM $MgSO_4$, 0.5 mM $CaCl_2$, 26.2 mM $NaHCO_3$, 72 mM sucrose and 22 mM glucose (equilibrated with 95% O_2 and 5% CO_2). The slices were incubated for 45 min in a submerged chamber at 34 °C containing the modified ACSF and kept in the same chamber at room temperature (20–25 °C) for 0 to 6 h before being placed in a recording chamber with normal ACSF at 31–33 °C.

Electrophysiology and analysis. Recorded neurons were visually identified using infrared differential interference contrast videomicroscopy. Unless stated otherwise, all whole-cell recordings were performed with patch pipettes (2–4 MΩ) filled with 150 mM potassium gluconate, 1.5 mM $MgCl_2$, 5 mM HEPES buffer, 1.1 mM EGTA and 10 mM phosphocreatine (pH = 7.25, 280–290 mOsm); biocytin (0.2% wt/vol) and 2 mM Mg-ATP were added in the recording solution for interneurons. When recording with a cesium-based intracellular solution, the composition was 115 mM cesium methanesulphonate, 8 mM NaCl, 10 mM HEPES, 0.3 mM Na_3-GTP, 4 mM Mg-ATP, 0.3 mM EGTA, 5 mM QX-314-Cl and 10 mM BAPTA tetracesium (pH = 7.4, 290 mOsm). Series resistance was not compensated but was monitored continuously with negative voltage steps, and recordings with series resistances larger than 12 MΩ were not included in the estimation of $EPSG_T$ in control conditions or after gabazine treatment. None of the additional recordings in the study had series resistances larger than 20 MΩ. Voltage measurements were not corrected for the experimentally determined junction potential (−11.7 ± 1.0 mV, $n = 3$). Experiments in the hippocampus were performed in the presence of the $GABA_B$ receptor antagonist CGP54626 (1–2 μM) and the NMDA receptor antagonist R-(−)-3-(2-carboxypiperazine-4-yl)-propyl-1-phosphonic acid (RS-CPP, 25–50 μM). The presence of the $GABA_B$ and NMDA receptor antagonists had no significant effect on the probability of eliciting a spike in pyramidal cells in response to threshold stimulation of Schaffer collaterals (CPP, 110.1 ± 11.9%; CGP54626, 119.8 ± 50.2%; $P = 0.84$ and 0.43, respectively).

Schaffer collaterals were stimulated (100 μs) with constant current (range of 10–900 μA) using a steel monopolar electrodes placed in the stratum radiatum of CA1. CA1 was isolated from CA3 and the subiculum by two radial cuts to prevent propagation of epileptiform activity. ChR2-expressing layer 2/3 pyramidal cells were activated by a full-field, 5-ms square light-pulse or 10-ms light-ramp from a 5-W luxeon blue LED coupled to the epifluorescence pathway of the Olympus BX51.

Loose-patch recordings were performed with ACSF-filled patch pipettes (8–10 MΩ). Field recordings were performed using patch pipettes (2–4 MΩ) filled with 3 M NaCl. Data were recorded with Axopatch 200A, Axopatch 200B or Multiclamp 700A amplifiers (Axon Instruments); acquisition (5–10-kHz digitization) and analysis was performed with pCLAMP 9.2 software (Molecular Devices). Average values are expressed as means ± s.e.m. Student's t test was used for statistical comparisons. We used 2,3-dihydroxy-6-nitro-7-sulfamoyl-benzo[f]quinoxaline-2,3-dione (NBQX), SR95531 (gabazine), CGP54626, RS-CPP, DAMGO, CTAP and muscimol (Tocris Cookson).

Calibrating input strength. The input strength is proportional to the number of activated Schaffer collaterals and varies from 0 to 1. It is a measure that allows comparison of stimulus intensities across slices. To estimate input strength, we used two experimentally determined parameters: the slope of the field EPSP (fEPSP), which is proportional to the number of activated Schaffer collaterals[41–43], and the amplitude of the population spike (population spike; **Supplementary Fig. 1**). Accordingly, all experiments in which the input strength is reported were performed in the presence of two field-potential recording electrodes, one placed in the stratum radiatum of CA1 (for fEPSPs) and one in the stratum pyramidale (for population spikes). The fEPSP was calibrated with respect to the simultaneously recorded population spike. Specifically, the slope of the fEPSP elicited at any given stimulus intensity was normalized by the slope of the fEPSP evoked at a stimulus intensity that evoked a population spike of 95% of its maximal amplitude (**Supplementary Fig. 1**). This normalization was done because even if the same number of Schaffer collaterals were recruited in two different slices, the absolute value of the slope of the fEPSP may vary (for example, as a result of a different positioning or depth of the recording electrode). The value of such normalized fEPSP is the input strength. Thus, the input strength is 1 when the number of stimulated Schaffer collateral triggers a population spike of 95% of its maximal amplitude and is 0.1 when the number of stimulated Schaffer collaterals is a tenth of the number it takes to trigger 95% population spike. For each slice, the input strength was always determined in control conditions. Thus, the number of Schaffer collaterals stimulated in control conditions or in gabazine is the same for a given input strength. In a subset of experiments, fEPSP was recorded in the stratum pyramidale. Experiments were only started once the amplitude of the population spike remained stable over a period of at least 10 min.

Threshold stimulation, activation curves and the measure of EPSCs and IPSCs peak amplitude, conductance and charge. Neurons were recorded in the loose-patch configuration and the Schaffer collaterals stimulated at increasing intensities until about 50% of the trials elicited a spike in the recorded cells. Neurons recorded in the loose-patch configuration were subsequently re-patched with a pipette containing standard internal solution (see above) to gain whole-cell access. In a subset of the recording reported in **Figures 1** and **2** (see legends), we determined threshold input strength using whole-cell recordings; the distribution of $EPSG_T$ with input strength did not differ significantly from the one obtained when threshold input strengths was determined in the loose-patch configuration (linear regressions, ANCOVA test on slopes, $P = 0.13$; intercepts, $P = 0.1$). The data were thus pooled.

The activation curve of a population of neurons (**Figs. 1a** and **5c**) is the cumulative distribution of the input strengths that elicit 50% spiking probability in the neurons of that population. The 50% spiking probability of individual neurons was interpolated by fitting their spiking probability plotted against stimulus strength (**Fig. 1a**) with the sigmoid function $Y = \frac{100}{1+10^{p(x_0-x)}}$, where x_0 is the input strength at 50% spiking probability and p is the slope at x_0.

Schaffer collaterals stimulation evoked an EPSC-IPSC sequence in pyramidal cells voltage clamped at about −60mV (**Supplementary Fig. 5**). To ensure that the recorded IPSCs were a result of the synaptic recruitment of GABAergic interneurons rather than of direct stimulation of inhibitory axons, we only considered experiments in which IPSCs could be abolished by the glutamate receptor antagonist NBQX[15] (at least 70% reduction, average of 84.4 ± 1.2%, $n = 50$; **Supplementary Fig. 5**). EPSCs were isolated by voltage clamping the pyramidal cell at the reversal potential of the IPSC (−88.9 ± 0.8 mV, $n = 43$). To estimate the amplitude of the EPSCs recorded at −60 mV (that is, well above the reversal potential of the IPSC), we used the amplitude of the EPSC recorded at the reversal potential of the IPSC after scaling its initial slope to the initial slope of the EPSC recorded at −60 mV (**Supplementary Fig. 5**).

The feedforward IPSC was isolated after subtracting the isolated and scaled EPSC from the EPSC-IPSC sequence. When present, the direct IPSC recorded in NBQX (never larger than 30% of the total IPSC amplitude, average 15.6 ± 1.2%, $n = 50$, see above) was also subtracted from EPSC-IPSC sequence. Peak synaptic excitatory and inhibitory conductances were computed as the peak of the EPSC or IPSC divided by the driving force at which the synaptic currents were recorded.

We can estimate the error on our EPSC measurement if the holding potential of the cell is ±10% off with respect to the actual IPSC reversal (say off by ± 8.5 mV if the IPSC reversal was −85 mV). The ratio between the peak of the $EPSG_T$ and the peak of the concomitant feedforward IPSG was approximately 1:0.8 (**Fig. 2**). Because of the 1.65-ms delay of the feedforward IPSC with respect to the onset of EPSC, at the peak of the EPSC the IPSC is only 55% of its maximal amplitude. Thus, with a driving force of 85 mV for the EPSC and a driving force of 8.5 mV

doi:10.1038/nn.2441

for the IPSC, the EPSC amplitude will be under- or overestimated by ± (0.8 × 0.55) × 0.1 = ±0.045. Thus, the error is below 5%.

The increase in feedforward inhibition with input strength (**Fig. 2a**) was fitted with the Boltzmann equation $Y = A - \frac{A}{1+e^{\frac{(x-x_0)}{p}}}$, where A is the asymptote, x_0 is the input strength at half maximal feedforward IPSG and p is the slope at x_0.

Correlation analysis of EPSC and IPSC amplitudes. The homogeneity of excitation (and inhibition) across the population of recorded neurons was accessed by correlating the average amplitude of EPSCs (or IPSCs) simultaneously recorded in cell pairs (**Fig. 4b**). These paired data can yield a range of different correlation values depending on whether each pair of amplitudes, A and B, is plotted as (A,B) (that is, A on the *x* axis and B on the *y* axis) or (B,A). To account for this, we repeatedly calculated the correlation where the dataset was the same, but each pair of amplitudes was randomly assigned to be (A,B) or (B,A). The mean correlation values from this process were $R = 0.3$ for EPSC pairs and $R = 0.8$ for IPSC pairs. The correlation between IPSCs was significantly larger ($P < 0.02$), assessed using one-tail test of correlation for dependent variables[44].

Anatomy. Slices containing neurons filled with biocytin were processed as described previously[21]. Neurons soma, dendrites and axons were reconstructed on a Zeiss light microscope (40×) using Neurolucida (MicroBrightField).

***In utero* electroporation.** Timed pregnant ICR white mice (Charles River) at embryonic days 15 and 16 were operated on as described previously[30]. Each embryo was injected with 1 μg of pCAGGS-ChR2-Venus[31] mixed with 0.5 μg of pCAG-EGFP.

Light-ramp versus light-pulse photostimulation. Light ramp–evoked EPSCs recorded in layer 5 pyramidal cells had a slower rise time as compared with light pulse–evoked EPSCs, consistent with the asynchronous recruitment of layer 2/3 pyramidal cells (1.3 ± 01 ms versus 2.4 ± 0.4 ms, $P = 0.03$, $n = 6$; **Fig. 6c**). To estimate the temporal distribution of the recruitment of layer 2/3 pyramidal cells, we deconvolved the asynchronous EPSC recorded in layer 5 pyramidal cells with the waveform of spontaneous EPSCs and computed the integral of the deconvolution. With the light ramp, the initial 50% of the activity generated in layer 2/3 occurred over a period of 7.4 ± 0.6 ms ($n = 6$), similar to the temporal distribution of spikes recorded in the somatosensory cortex *in vivo* in response to a whisker stimulus[7].

Computational model. We sought to design a simple model constrained by experimentally determined parameters (anatomical connectivity and average number of inputs required to reach threshold) to establish whether the experimentally measured increase in $EPSG_T$ can, in principle, account for the observed dynamic range of the activation curve. Our model predicts the fraction of pyramidal cells activated as a function of the number of active Schaffer collaterals, given a connectivity p of Schaffer collaterals onto pyramidal cells. We assume that all Schaffer collateral-pyramidal cell synapses have the same strength. Thus, the distribution of inputs strengths onto the pyramidal cell population is given by the binomial probability distribution.

Accordingly the fraction A of active pyramidal cells given N active Schaffer collateral is

$$A_N = 1 - \sum_{i=0}^{T} \binom{N}{i} p^i (1-p)^{N-i}$$

where N is the number of Schaffer collaterals, and T is threshold of excitation expressed in terms of the number of active presynaptic inputs *i*. p is taken as 0.06 (ref. 25), and the fixed $EPSG_T$ activation curve was simulated using a constant threshold, $T = 100$ (ref. 2). To simulate the dynamic $EPSG_T$ activation curve, the threshold was 100 Schaffer collaterals initially, but changed as a function of input strength, $T(N)$, optimized to minimize the distance between the simulated and experiment activation curves. This optimization was constrained by our experimental finding such that it increased by ~threefold, reaching a plateau when ~65% of the pyramidal cells were active (Matlab, Mathworks).

41. Vaillend, C., Mason, S.E., Cuttle, M.F. & Alger, B.E. Mechanisms of neuronal hyperexcitability caused by partial inhibition of Na+-K+-ATPases in the rat CA1 hippocampal region. *J. Neurophysiol.* **88**, 2963–2978 (2002).
42. Nakamura, M., Sekino, Y. & Manabe, T. GABAergic interneurons facilitate mossy fiber excitability in the developing hippocampus. *J. Neurosci.* **27**, 1365–1373 (2007).
43. Winegar, B.D. & MacIver, M.B. Isoflurane depresses hippocampal CA1 glutamate nerve terminals without inhibiting fiber volleys. *BMC Neurosci.* **7**, 5 (2006).
44. Steiger, J.H. Tests for comparing elements of a correlation matrix. *Psychol. Bull.* **87**, 245–251 (1980).